https://doi.org/10.5194/egusphere-2026-1823
Preprint. Discussion started: 4 June 2026

Interannual variability of the winter sea ice edge in the Southern Ocean tuned by topography and oceanic transport.

Hugues Goosse[1], Cecile Davrinche[1], Benjamin Richaud[1], Dániel Topál[1], Stephy Libera[1], Alberto C. Naveira Garabato[2], Alessandro Silvano[2], Martin Vancoppenolle[3] , Pablo Ortega[4]

[1]Earth and Life Institute, Université catholique de Louvain, Louvain-la-Neuve, Belgium
[2]Ocean and Earth Science, National Oceanography Centre, University of Southampton, Southampton, UK.
[3]Sorbonne Université, Laboratoire d'Océanographie et du Climat (LOCEAN-IPSL), CNRS/IRD/MNHN, Paris, France
[4]Barcelona Supercomputing Center, Barcelona, Spain.

Corresponding author: Hugues Goosse (hugues.goosse@uclouvain.be)

Abstract

The large-scale interannual variability of sea ice concentration in the Southern Ocean is largely controlled by atmospheric dynamics. By contrast, based on satellite observations, we show here that the local amplitude of interannual variations of the winter sea ice edge position is mainly modulated by the ocean bottom topography and oceanic processes. The standard deviation of the latitude of the ice edge displays substantial variations as a function of longitude, with prominent sharp peaks covering only a few degrees of longitude close to the main topographic features of the Southern Ocean. There, mesoscale eddy activity and the variability of the Antarctic Circumpolar Current jets are large, influencing both oceanic heat transport and sea ice velocity, thereby leading to large interannual changes in the position of the ice edge. Owing to such bathymetric control, these regions showing high variability in the winter ice edge position have remained relatively stable over recent decades, despite ample changes observed in other characteristics of the sea ice cover during the same period. Eddy-rich global sea ice-ocean models based on NEMO-SI3, both forced by ERA5 surface fluxes or coupled with the atmospheric model IFS, can reproduce the sharp peaks in the variability of the ice edge position, indicating that they adequately simulate the dominant influence of topography on currents and eddy activity. However, this requires a realistic mean ice edge position; otherwise, model biases can displace the ice edge away from regions of strong eddy activity and therefore distort the interannual variability.

1. Introduction

The total Antarctic sea ice extent has significantly decreased over the past decade, after a period of relative stability between 1979 and 2015 (Parkinson and DiGirolamo, 2021; Purich and Doddridge, 2023). This general trend of the ice coverage over the Southern Ocean is embedded in a large interannual variability (see Hobbs et al., 2016; Ears et al., 2019 for reviews). The magnitude of interannual variability, as measured by the standard deviation of Antarctic sea ice extent, is larger during spring and autumn and weaker in summer and winter (Parkinson, 2014; Zunz et al., 2013; Hobbs et al., 2016). The relatively low variance in winter may seem surprising given that the total ice extent is much larger than in other seasons. However, model studies have indicated that the variance increases with the mean ice extent in summer (Goosse et al., 2009) whereas in winter it increases only if the ice extent is lower than about 10 10^6 km^2, far below the currently observed value (Diamond et al., 2024). The variance of the sea ice extent also changes with time (Li and Wu, 2020; Hobbs et al., 2024), with the recent increase in variance and persistence being considered as one argument in favor of a regime shift (Hobbs et al., 2024).

Most studies to date have analyzed variability in sea ice extent for the Southern Ocean as a whole or separated in a few sectors. Large-scale modes of sea ice variability have also been identified, based directly on the sea ice concentration fields or through connections with atmospheric modes of variability (e.g., Yuan and Martinson, 2001; Parkinson and Cavalieri, 2012). In particular, key elements of the spatial variability in ice cover have been linked to dominant modes of variability in the Southern Hemisphere, including the Southern Annular Mode (SAM), El-Niño Southern Oscillation (ENSO) and the Zonal Wavenumber 3 (ZW3) mode (e.g., Raphael, 2007; Stammerjohn et al., 2008; Lefebvre and Goosse, 2008; Eabry et al., 2025; Boehm et al., 2025). The different phases of these modes are associated with changes in atmospheric meridional heat transport, surface heat fluxes and surface wind stress (which in turn affects sea ice transport and oceanic currents), thereby contributing to variations in sea ice concentration and in the position of the ice edge.

In contrast to these large-scale changes, the variability of the ice edge position on scales of a few hundred kms has received less attention. However, the interannual shifts at specific locations can be much larger than averaged over a sector covering 50 to 100° of longitude, as illustrated by some of the recent extremes (Purich and Doddridge, 2023; Espinosa et al., 2024). Understanding those smaller-scale variations is important for better characterizing the interannual variability of sea ice cover, more clearly distinguishing long-term trends from interannual fluctuations, and improving regional to local sea ice predictions (Massonnet et al., 2023; Zhao et al., 2024).

A classical view attributes a dominant role of atmospheric processes in explaining interannual variations of the ice cover, whereas the ocean may contribute more importantly on longer timescales – including in the recent shift towards a lower sea ice extent (Bitz, 2005; Ferreira et al., 2015; Hobbs et al., 2016; Purich and Doddridge, 2023; Silvano et al., 2025, Spira et al., 2026; Wilson et al., 2026). However, the mean position of the ice edge is shaped by oceanic processes. Specifically, the pathway of the Antarctic Circumpolar Current (ACC) influences the mean position of the winter ice edge, directly through its impact on meridional heat transport by ocean currents and eddies as well as indirectly by modifying atmospheric transport (Martinson, 2012; Goosse et al., 2025). As the path of the ACC itself is controlled by the bottom topography (e.g., Rintoul, 2018), the position of the ice edge reflects the underlying bathymetry of the Southern Ocean. Oceanic processes may also modulate the interannual variability of the ice cover, for instance through a strong localized impact of large-scale oceanic currents or of mesoscale eddies in the vicinity of major topographic features. This possibility remains largely unexplored at present, except in a few specific regions (e.g., Ferola et al., 2023).

The goal of this paper is to evaluate the processes in explaining the interannual variability of the Antarctic sea ice edge position in observations as well as in ice-ocean and coupled climate model simulations. It comes in complement with our recent paper showing that the path of the Antarctic Circumpolar Current has a large influence on the mean position of the ice edge (Goosse et al., 2025). Here we analyze interannual variations in the winter ice edge based on the September monthly mean. September is of particular interest because it corresponds to the annual maximum in sea ice extent. September is also well suited for illustrating the contribution of oceanic processes, whose impact is likely to be substantial at the end of winter (e.g. Martinson, 1990). Additionally, previous studies have indicated that climate models generally overestimate winter sea ice variability (Zunz et al., 2013; Roach et al., 2020). As an auxiliary objective, we investigate whether higher horizontal resolution, and thus a better representation of bathymetry-driven oceanic processes and mesoscale eddies, reduces this bias both for the local variability of the ice edge position and at larger scales.

2. Methods

2.1. Observations

Sea ice concentration observations since 1979 are taken from EUMETSAT OSI SAF (OSI-450 and OSI-430-b; OSI SAF 2017; Lavergne et al., 2019). The winter sea ice edge is defined as the 15% ice concentration contour based on the algorithm of Eisenman (2010). The sea ice edge is first interpolated to a 1° horizontal resolution before diagnostics are performed. 10-m wind speed is derived from the ERA5 reanalysis (Hersbach et al., 2020a). Monthly mean ocean geostrophic velocities are obtained from Dragomir (2024) who calculated them from dynamic ocean topography observed from satellites between July 2002 and October 2018. The eddy kinetic energy over the Southern Ocean has been reconstructed by Auger et al. (2022) for the period 2013 to 2019 using sea level anomaly from multiple satellite sources. The bathymetry is obtained from ETOPO1 (Amante and Eakins, 2009). The Polar Pathfinder Daily 25 km EASE-Grid Sea Ice Motion Vectors, Version 4 provides the sea ice velocity for the period 1979-2023 (Tschudi et al., 2019). The definition of the Polar Front follows that of Park et al. (2019), based on the selection of a circumpolar sea surface elevation contour that matches the observed position of the Polar Front in key regions for the 1993-2012 period. Those products cover different time intervals but we assume that each of them is long enough to represent a climatological average (see also the discussion in section 3b).

2.2. Model results

We analyze high-resolution simulations performed with the ocean-sea ice model NEMO (Nucleus for European Modelling of the Ocean) in two configurations, either driven by the ERA5 reanalysis or coupled to the IFS atmospheric model. An additional set of high-resolution coupled atmosphere-ocean model simulations is also presented in the Supplement. As atmospheric forcing is constrained by observations (including sea ice concentration) in the reanalysis, the NEMO model driven by ERA5 is expected to follow the observed variations. Because of the absence of atmosphere-ocean feedbacks in this standalone configuration, it is not always possible to disentangle the contribution from oceanic processes in the simulated fields from those imposed directly by the atmospheric forcing (e.g. Goosse et al., 2023). By contrast, the fully coupled simulations include all the relevant feedbacks but, as they are not constrained by observations, they could present significant biases and uncertainties due to a different sampling of internal variability. Thus, the two types of simulation provide complementary information.

The NEMO model (Madec, G. and the NEMO System Team, 2023) includes OPA (Océan PArallélisé) as its ocean component and SI^3 (Sea Ice modelling Integrated Initiative) as its sea ice component (Vancoppenolle et al., 2023). For the ERA5-driven simulation, we use NEMO4.2 as in Richaud et al. (2026) at a horizontal resolution of 1/12° based on the eORCA12 global tripolar grid. It covers the period 1995-2024. A simulation with the same version of NEMO driven by ERA5 but at 1° resolution is also used in the Supplement to estimate the influence of the resolution. Additionally, we analyze the last 30 years (1985–2014) of a historical simulation performed with the coupled model IFS-NEMO-ER, the eddy-rich configuration developed within the EERIE, nextGEMS and Destination Earth projects (Rackow et al., 2025; Doblas-Reyes et al., 2026). The simulation corresponds to a hist-1950 experiment from the High Resolution Model Intercomparison Project (HighResMIP; Haarsma et al., 2016; Roberts et al., 2025) and was initialized from a 60-year spin-up under fixed 1950 forcing. The simulation is driven by historical radiative forcings from CMIP6 (Eyring et al., 2016), with the exception of tropospheric aerosol forcing, which is prescribed as a time-evolving climatology derived from IFS simulations with prognostic atmospheric chemistry from CAMS. IFS-NEMO-ER combines version 4.0.7

of NEMO and SI^3 (Madec et al., 2019, Vancoppenolle et al., 2023) with an EERIE-revised build of cycle 48r1 of the atmospheric model IFS (DE_CY48R1.0_EERIE_20240726). The atmospheric component uses a Tco1279 Gaussian octahedral grid (~9 km horizontal resolution) with 137 vertical levels, while the ocean-sea ice system is configured on an eORCA12 global tripolar grid (~1/12° resolution) with 75 vertical levels, as in the atmosphere-forced configuration. Importantly for this study, a modified air-sea ice coupling strategy is employed. Rather than relying on the default IFS sea ice surface treatment, where atmospheric fluxes are computed using an internal IFS sea ice module and sea ice concentrations from SI^3, IFS directly computes air–ice fluxes from sea ice properties provided by SI^3, including sea ice concentrations, surface temperature, and albedo. The IFS sea ice module is therefore disabled. This physically more consistent coupling avoids known imbalances in the surface energy budget that can otherwise lead to unrealistically sustained sea ice growth and numerical instabilities, and is particularly relevant for an accurate representation of the winter sea ice edge in the Southern Ocean.

3. Results

3.1. Local variability of the ice edge as a function of longitude

3.1.1 Observed variability of the winter ice edge and its link with topography

The most northward and southward positions of the winter ice edge over the period 1979-2025 are separated by only a few degrees at most longitudes (Fig. 1a), but a closer look indicates that this range strongly varies across regions. This difference between regions is confirmed by the temporal standard deviation of the winter ice edge latitude's interannual variability as a function of longitude (Fig. 1b), which has a spatial mean of 1.0° and a standard deviation of 0.2° over all longitudes. Local values can be much larger or lower than the mean; for instance, the temporal standard deviation of the winter ice edge latitude is larger than 1.5° around 30°E or 220°E, while it is lower than 0.5 at 175°E.

The local winter ice edge interannual variability is much larger than that of the total sea ice extent because each year is characterized by a specific pattern in which changes in one region is partly compensated by changes in another in the integrated view. For a point of comparison, a band of one degree of latitude at 60°S is associated with a surface area of 2.2 10^6 km^2. The standard deviation of the ice extent in winter reaches 0.5 10^6 km^2 over the period 1979-2025 (estimated here from EUMETSAT OSI SAF). If we make a simple scaling and distribute this standard deviation around all longitudes at 60°S, it would then correspond to a mean shift of about 0.2°, i.e. 5 times less than the mean of the standard deviations of the winter ice edge latitude given above.

Remarkably, the standard deviation of the winter ice edge latitude is not spatially smooth, but shows sharp, narrow peaks often confined to only a few degrees of latitudes (Fig. 1b). The main peaks for the period 1979-2025 are located in the longitude bands 13-28°E, 78-81°E, 101-104°E, 149-154°E, 210-230°E, 267-270°E, 302-320°E, and 327-332°E. Most of these peaks are narrower than 10° and several are narrower than 5° (specifically, at the resolution used here, the band between 302-320° is interrupted by two longitudes exhibiting relatively lower standard deviation). This feature strongly contrasts with the relatively smooth mean position of the ice edge (Fig. 1a).

All the peaks in the standard deviation of the ice edge position are located close to the main topographic obstacles (Fig. 1a) along the path of the Antarctic Circumpolar Current: 13-28°E near Bouvet Island and the western part of the Southwest Indian Ridge, 78-81°E and 101-104°E near Kerguelen Plateau, 149-154°E near the Southeast Indian Ridge, 210-230°E near the Pacific Antarctic

Ridge, and 302-320°E and 327-332°E on the Scotia ridge and South Sandwich Arc. Although the region between 267° and 270°E is not in the vicinity of a major ridge system, some topographic obstacles are still present close by, such as the De Gerlache seamounts (270°E 65°S), which are located just north of the mean ice edge position at that longitude.

3.1.2 Stability of the magnitude of interannual variability between different periods

While many climatic changes have occurred recently in the Southern Ocean, the longitudinal variations of the standard deviation of the winter ice edge position remain very similar if we split the period covered by satellite observations into two consecutive time intervals of (nearly) equal duration (1979-2002 and 2003-2025). Changes are observed, and some smaller peaks appear or disappear between the two periods, but the main peaks identified for the full interval remain at exactly the same locations (Fig. 1b). The correlations between each of the sub-periods and the full 1979-2025 period are higher than 0.85 in both cases (the correlation between the two sub-periods is 0.52). Even if we specifically target the last decade (2016-2025), which is characterized by a decrease of the sea ice extent and an increase of its variability and persistence (Purich and Doddridge, 2023; Hobbs et al., 2024; Raphael et al., 2025), we do not find major modifications for the standard deviation of the ice edge position (Fig. 2b). As only 10 years are analyzed, the curve is a bit noisier for the period 2016-2025, resulting is a correlation with the curve for the whole period of 0.68, but nearly all the peaks observed for the full period are also present (the correlation between the standard deviation over the periods 1979-2015 and 2016-2025 is 0.52). The main difference in the most recent period is the lower standard deviation of the ice edge position between 60 and 150°E compared to the period 1979-2025, and specifically the absence of the double peak in the Kerguelen region which corresponds to the longitude with the largest retreat of the winter ice edge in 2016-2025 (Fig. 2a). It is thus possible that the southward shift in the position of the ice edge distances it from the main bathymetric obstacles, leading to lower interannual variability. A decrease of the standard deviation is also seen close to the west Antarctic Peninsula (between 300 and 320°) where the winter ice edge has also retreated and remains very close to the coast during some years. Overall, these relatively small differences suggest that the processes responsible for the local variability of the ice edge have not changed much over recent decades, and that the ongoing sea ice decline is associated with mechanisms different from those responsible for the local interannual variations of the ice edge position.

3.1.3 Simulated variability of the winter ice edge

The observed longitudinal variations of the standard deviation of the ice edge position are well reproduced by the 1/12° horizontal resolution standalone ocean-sea ice simulation (i.e., NEMO forced by ERA5), with a correlation of 0.73. In particular, the model simulation mirrors most of the sharp peaks located close to the main bathymetric elements (Fig. 3). This simulation precludes disentangling the contribution of oceanic processes from the direct effects of the atmospheric forcing, which is itself constrained by the observed variability of the ice cover. Nonetheless, the same standalone simulation configured at a coarser resolution (1°) does not display the sharp peaks identified at high resolution, even though both diagnostics are compared at the 1° resolution (Fig. S1). As a consequence, the correlation of the longitudinal variations of the standard deviation of the ice edge position with observations is lower in this 1° configuration than in the high resolution version, with a value of 0.58 - while the mean position is well reproduced in both cases (correlations higher than 0.95). Therefore, increased horizontal resolution is key for adequately reproducing the observed features, which hints at an important role of topography and small-scale oceanic processes in controlling the local variability of the ice edge.

The differences between the observed and simulated standard deviations of the ice edge position are also instructive, as they indicate regions where the model is biased despite the ERA5-constrained atmospheric forcing. This model-observation disagreement is largest downstream of the Kerguelen Plateau between 90 and 140°E, where NEMO driven by the ERA5 reanalysis shows a pronounced minimum in ice edge variability (Fig. 3). In this region, the mean simulated ice edge is located several degrees to the south of the observed one. As argued to tentatively explain the changes observed over the period 2016-2025 in the above sub-section, this moves the ice edge away from the main bathymetric features that underpin oceanic variability. By contrast, the underestimation of the ice extent between 220° and 280°E is not associated with any bias in the magnitude of the simulated variability, except for the small peak at 270°E. There is no main oceanic ridge in this sector and a shift in the ice edge position seems then to have a smaller impact on its variability. Underestimation of the variability is also present between 180 and 200°E, as well as close to the Antarctic Peninsula between 300 and 320°E, despite a simulated sea ice edge that is near the observed one.

Using a coupled atmosphere-ocean-sea ice model releases the constraint on the variability brought by the forcing in the simulation with NEMO driven by ERA5. This comes with the risk of larger biases, but IFS-NEMO simulates an ice edge that is close to the observed one (with a correlation of 0.97), except an overestimation of the ice extent between 0 and 110°E (Fig. 3a). The standard deviation of the ice edge position is also close to the observed one in most sectors and the variance of the ice extent in September (0.54 10^6 km^2) is in good agreement with the observed one (0.51 10^6 km^2) and with that of NEMO forced by ERA5 (0.50 10^6 km^2).

The main biases in the standard deviation of the ice edge position simulated in IFS-NEMO are the smaller and shifted peak compared to the observed one between 13 and 28°E, and the much larger peak at 100°E. These peaks are in the regions where the difference between the observed and simulated ice edge positions is the largest. By contrast, the small peak at 270°E is very well simulated, as the ice edge position is closer to the De Gerlache seamounts than in NEMO driven by ERA5, which misses this peak. In the longitude bands of 180-200°E and 300-320°E, the simulated variability in IFS-NEMO is closer to that of NEMO forced by ERA5 than to the observations, despite a realistic position of the ice edge in both models. This suggests that those biases in the variability are not linked to the atmospheric forcing, but most probably to the inability of the ocean model to adequately represent the effect of the bathymetry despite the model's relatively high resolution – in particular the complex bathymetry close to the tip of the Antarctic Peninsula with multiples channels and islands. Overall, despite the qualitative agreement on the location of most peaks, the correlation of the longitudinal variations of the standard deviation of the winter ice edge position in NEMO-IFS with observations is only 0.15, because of those biases and the differences in the magnitude of the peaks. The correlation is higher (0.45) if we compute it over the longitudes 150-360, i.e. the regions where the mean state of NEMO-IFS is closer to observations.

The relatively good qualitative agreement with observations obtained from IFS-NEMO can plausibly be related to the high resolution of the model, which is required to reproduce the local variability and in particular the effect of the bathymetry. However, high resolution is by itself not sufficient, as illustrated for three other high-resolution models (Sup Fig. 2) that display large biases in their representation of the mean sea ice edge position. Nevertheless, in the sectors where the simulated ice edge is close to the observed one in those three models, the standard deviation of the ice edge position display peaks at the same locations of the observed ice edge. This suggests that the presence of the peaks is not specific to the selection of the model, configuration, or to atmospheric or oceanic variability patterns (which are different between the forced and coupled simulations), rather to a more robust constraint present in the coupled and uncoupled configurations – such as that provided by the bathymetry.

3.2. Processes driving the local variability of the ice edge

In section 3.1, we have identified, in observations and models, robust peaks in the standard deviation of the winter ice edge position that we have related to the topography of the Southern Ocean. In this section, we investigate the processes through which such an influence of the topography may be exerted.

3.2.1 Role of the winds

Fig 4. shows meridional winds at 10-m and their standard deviations at 60°S, which is close to the mean location of the winter ice edge (similar results are obtained if we use instead the winds at the latitude of the ice edge). From both the climatological mean meridional winds and their standard deviation, there is no indication that winds would have a significant impact on the standard deviation of the winter ice edge position. The correlation between the standard deviation of the winter ice edge position and both the mean and standard deviation of the meridional winds is very close to zero (-0.04 and 0.04, respectively). Hence, neither stronger southerly winds such as those between 40 and 80°E, nor stronger northerly winds such as those around 150°E, are associated with systematically larger or smaller variations in ice edge position. Similarly, a relatively larger standard deviation of the meridional wind component between 250° and 300° corresponds to a modest variability of the ice edge position in most of this sector. Additionally, the typical length scale of variations in meridional wind speed and its standard deviation is several tens of degrees, which far exceeds the one of standard deviation of the sea ice edge characterized by narrow peaks.

Here we use meridional winds as a proxy for the potential impact of the atmospheric circulation on the sea ice edge position on interannual timescales, as many studies have indicated a clear link between this variable and the Southern Ocean temperature or sea ice extent (e.g., Bitz et al. 2005; Raphael, 2007; Lefebvre and Goosse, 2008; Haumann et al., 2016; Kwok et al., 2017; Blanchard-Wrigglesworth et al., 2021; Kusahara and Tatebe, 2025, Edholm et al. 2025; Goosse et al.; 2025). Other elements of atmospheric circulation also display variations between the different sectors of the Southern Ocean, such as the position of the storm tracks or atmospheric eddy activity, which is stronger over the eastern South Atlantic and Indian oceans. However, as the winds, they display variability on much larger spatial scales than those of sea ice edge changes, and no strong correspondence with the peaks in sea ice edge variability is apparent (Nakamura and Shimpo, 2004; Zhan et al., 2023; Zhang et al., 2024).

There is no doubt that atmospheric circulation affects the mean position of the ice edge and its variability as demonstrated, for instance, by the large number of studies relating sea ice concentration and atmospheric modes of variability (Raphael, 2007; Stammerjohn et al., 2008; Lefebvre and Goosse, 2008; Boehm et al., 2025) or by studies that identify a dominant atmospheric trigger of the recent major winter sea ice anomalies (Turner et al., 2017; Schlosser et al., 2018; Jena et al., 2024; Wang et al., 2024). However, while those studies documented the impact of atmospheric circulation on the spatial pattern of the sea ice changes, the local magnitude of those changes, as measured by the standard deviation of the position of the ice edge, seems rather disconnected from atmospheric circulation. The main processes explaining the magnitude of the local sea ice edge variability in winter (Fig. 1) thus originate from the ocean, as discussed below.

https://doi.org/10.5194/egusphere-2026-1823
Preprint. Discussion started: 4 June 2026

3.2.2 Influence of the Polar Front

Oceanic processes can influence the ice edge position variability in different ways. First, north of the sea ice zone, the strong thermal gradients of the ACC exert a natural barrier for the expansion of the Antarctic sea ice extent (Goosse et al., 2025). Consequently, the position of the Polar Front could limit the variability of the ice edge, but this is seen only in some regions of the Pacific sector and in the western Weddell Sea. The impact is visually striking between 270°E and 310°E, i.e. east and west of Drake Passage, where the maximum northern position of the ice edge exactly corresponds to the position of the Polar Front (Fig. 1a). This indicates that sea ice can reach the front during some extreme years in this sector, but it melts rapidly before it can cross the front. Note that the definition of the front used in Park et al. (2019) is based on sea surface elevation, thus it is only indirectly connected to the water mass characteristics and to the temperature gradient that blocks sea ice expansion. Despite the strong northward limit imposed by the Polar Front, the standard deviation of the ice edge position is not particularly low between 270º and 310º: the climatological mean position of the ice edge is still located far enough of the front to allow large amplitude fluctuations, except to some extent at 280°E (Fig. 1b, Fig. 5a). The situation is different at 170°E, where the maximum sea ice edge position reaches the Polar Front. The Polar Front is at one of its most southern positions and is very close to the mean ice edge (Roach and Speer, 2019; Ferola et al., 2023, Goosse et al., 2025); This strongly restricts sea ice expansion in winter nearly every year, and not only in extreme years, as it is the case close to Drake Passage, leading to the lowest standard deviation of the ice edge position among all longitudes (Fig. 5a). In other sectors, the Polar Front appears to lie too far away from the sea ice edge to have a direct influence on the local ice variability, in contrast to the front's impact on the climatological mean position of the ice edge (Goosse et al., 2025). As a consequence, despite these local impacts in some sectors, the overall correlation between the standard deviation of the ice edge position and the distance between the mean ice edge and the Polar Front is very low (0.07).

3.2.3 Role of the oceanic eddies

Second, nearly all the peaks in the standard deviation of the ice edge position are located close to the regions of strong mesoscale eddy activity (Fig 5b, Fig. 6) that results from the interactions between the Antarctic Circumpolar Current and the main topographic obstacles identified in Fig. 1. (Sallée et al., 2011; Thompson and Sallée, 2012; Rintoul, 2018). The strong link between eddy activity and ice edge variability could be explained by a large contribution of eddies to the meridional heat transport in the Southern Ocean (Sallée et al., 2011; Thompson and Sallée, 2012; Dufour et al., 2015; Morison et al., 2016; Hausmann et al., 2017; Rintoul, 2018, Ferola et al., 2023). As the regions showing strong eddy activity are also regions of large meridional heat transport, the variability of meridional heat transport has a large imprint on the heat balance at the sea ice edge, and thus on the variability of its position. Note that the variance of eddy kinetic energy has a similar pattern as the mean of eddy kinetic energy shown in Fig. 5b, but we prefer to display the mean here because of the shortness of the available dataset. The simulations with NEMO driven by ERA5 and IFS-NEMO also display a strong correspondence between the peaks in eddy kinetic energy and in the standard deviation of the ice edge, illustrating the robustness of the link in models too (Fig. S3).

While nearly all the regions with a large variability of the sea ice edge position are characterized by large eddy activity, some locations with large eddy activity display modest or weak variability in the ice edge position. The clearest case is at 170°E. As discussed above, the Polar Front is closer to the mean ice edge there. The position of the fronts and the large eddy-induced heat transport both strongly limit each year's northward ice expansion, and thus the variability of the ice edge. Similar processes explain the double peak in the standard deviation of the ice edge seen close to the Kerguelen Plateau (at 78-81°E and 101-104°E). The peak in eddy activity is between those two peaks at 85°E, but the variability

https://doi.org/10.5194/egusphere-2026-1823
Preprint. Discussion started: 4 June 2026

of the ice edge is low at 85°E because of the strong eddy activity at higher latitudes, which limits the expansion of the ice edge at that particular location. Indeed, the maximum position of the ice edge closely follows the region with high eddy activity in the Kerguelen area, with a clear inflection of the northernmost position of the ice edge at 85°E (Fig. 6). In addition, the local maximum of the eddy kinetic energy is close to the mean ice edge at both 85°E and 170°E (Fig. 5b; defined here as the mean eddy kinetic energy averaged in the region, which is maximum 2° north of the mean ice edge position). In other words, a high eddy kinetic energy can be viewed as a double-edged sword. Without eddies, the variability of the oceanic heat transport and of the ice edge position are small; but if the eddy activity at high latitudes is too large, the associated heat transport sufficiently constrains ice expansion and thus limits its variability.

The correlation between the eddy kinetic energy and the standard deviation of the ice edge over all longitudes reaches only 0.13. This is due to the few regions with high eddy activity and low standard deviation of the sea ice edge position (85°E and 170°E), and to the presence of some shifts in the longitude between the peaks in these two variables (such as the peak in eddy kinetic energy at 40°E shifted compared to the large standard deviation of the ice edge between 13-28°E). The correlation increases a little, up to 0.28, if a 15° smoothing is applied to both spatial series to partly consider that eddies can propagate and affect the ice edge at nearby longitudes. However, the agreement is much larger if we focus only on half of the domain (between 180°E and 360°E; i.e. avoiding the regions of lower correspondence at 40°E, 90°E and 170°E) with a correlation reaching 0.57 (0.77 after the 15° smoothing).

3.2.4 Role of oceanic currents

Third, large-scale ocean currents also contribute to the horizontal heat transport and may thus affect the position of the ice edge. Consequently, regions exhibiting elevated variability in oceanic flows could also bring about a large standard deviation of the winter ice edge position. This influence is estimated in Fig. 5c using the meridional geostrophic velocity derived from monthly mean sea surface elevation (Dragomir, 2024). Peaks in the standard deviation of the geostrophic velocity are found roughly in the same regions as the eddy kinetic energy (Fig 5b) as the topography influences both the mean currents and the mesoscale activity, with for instance large standard deviations near the Kerguelen Plateau, at 175°E and at Drake Passage. The difference between the regions is smaller for the standard deviation of the geostrophic velocity than for the eddy kinetic energy, and the correlation between the standard deviation of the geostrophic velocity and the standard deviation of the ice edge position is low when applied to all the longitudes (0.18). Nevertheless, a clear maximum in the standard deviation of the geostrophic velocity is present at 30°E and coincides exactly with the local maximum in the standard deviation of the ice edge. The standard deviation of the geostrophic velocity is also relatively high at 270°E, a region of high variability of the ice edge position but of no clear maxima in the eddy kinetic energy. Consequently, the correlation between the standard deviation of the geostrophic velocity and the standard deviation of the ice edge position over the region between 0 and 50°E reaches 0.49 (with 0.64 between 20 and 40°E, and 0.48 for the region between 260 and 280°E). However, these are relatively small areas. Correlation can be opposite for several other regions of the same size, and the power of the statistical test is highly questionable as we choose these regions on the basis of the visual agreement in Fig. 5c. Besides, a link is also found between the mean meridional geostrophic velocity and the standard deviation of the ice edge, but it is likely due to a common influence of topography on both (see the Supplementary Discussion).

3.2.5 Role of sea ice velocity

Close to the ice edge, sea ice dynamics can be a dominant term in the mass balance of the ice pack (e.g., Bitz et al., 2005; Holland and Kimura, 2016; Himmich et al., 2023). Indeed, some of the local maxima in the standard deviation of the meridional sea ice velocity and in the position of the winter ice edge are in the same longitude bands, such as 78-81°E, 149-154°E, 210-230°E, 267-270°E and 327-332°E (Fig. 5d). However, a systematic link between the variability of the meridional sea ice velocity and the ice edge variability could not be identified. The correlation between those two variables is close to zero.

The peaks in the standard deviation of the ice velocity are on spatial scales similar to the ones of the peaks in eddy kinetic energy and mean oceanic velocity, but on much smaller spatial scales than those associated with atmospheric variability. This advocates for a dominant contribution of ocean processes as, for instance, eddies can influence sea ice transport through their signature in ocean surface currents and by sea ice trapping in eddies (Manucharyan and Thompson, 2017; Cai et al., 2025).

4. Conclusion

We analyzed the interannual variability of the winter ice edge position in the Southern Ocean, and identified large peaks in the ice edge's standard deviation over a few narrow longitude bands. The drivers of these sharp peaks in the ice edge variability contrast with those of the larger-scale patterns of sea ice cover changes. Despite the key role of atmospheric processes on these large-scale patterns, the local amplitude of the variations of the position of the winter ice edge from year to year is largely controlled by oceanic processes, and specifically by oceanic processes shaped by bathymetry. Major ridge systems influence the path of the currents and the formation of mesoscale eddies, consequently affecting the oceanic heat transport and sea ice velocities that then tune the magnitude of the local changes in the ice edge position. This induces a larger variability of the winter ice edge position close to these ridge systems.

As the variability of the ice edge position is strongly constrained by the bathymetry, its magnitude has been relatively stable over recent decades, despite recently observed sea ice changes (Parkinson et al., 2021; Purich and Doddridge, 2023; Hobbs et al., 2024). A coupled atmosphere-ocean model, and the same ocean model driven by an atmospheric reanalysis – both with an adequate resolution to represent the bathymetric constraint and associated oceanic processes – can reproduce the observed positions of peaks in the standard deviation of the ice edge. As the sea ice is driven by different evolution of atmospheric fields in the two model configurations, this confirms that such peaks are not dependent on the specific atmospheric conditions observed over past decades, or on recent atmospheric and ice trends. Nevertheless, the mean position of the ice edge has a clear importance, as a small shift or bias in the model may move the ice edge away from the key bathymetric features, invalidating the controlling influence of topographically generated oceanic processes in the high ice edge variability. To credibly reproduce the ice edge variability, the models must realistically simulate the mean state of the ice cover. In that case, it is possible to have both a good representation of the local magnitude of the variability and of the variability of the ice extent in winter, avoiding the overestimation found in many coupled climate models for the latter (Zunz et al., 2013; Roach et al., 2020).

While the conclusion on the first-order role of topography is clear, a precise quantification of the contributions of the various processes that influences the variability of the ice edge position is complex. Differences are present amongst the different longitudes and the statistical evidence is less straightforward than for the mean position of the winter ice edge (e.g., Goosse et al., 2025). Overall, there is good correspondence between the regions of high eddy activity around topographic barriers on the ACC flow and the regions of high variability in the ice edge position, especially between 180 and 360°E. However, there are exceptions to this view. First, between 13 and 28°E, the peak in the ice edge variability is located eastward of a peak in eddy kinetic energy. Besides, it is exactly at the same longitude as a peak in the standard deviation of meridional geostrophic velocity, arguing for a dominant role of the larger scale currents at this location. Second, a local disagreement between peaks in eddy activity and ice edge variability is found at 85° and 170°E, where large eddy activity is associated with a low standard deviation of the ice edge position. At both longitudes, eddy activity is intense even at latitudes close to the mean ice edge. This could induce large heat transport that strongly restricts the advance of the ice edge each year and thus its variability. Additionally, the Polar Front exerts a natural northern limit to the mean sea ice edge position. If the front is located close to the mean ice edge, such as at 170°E, it restrains the northward progression of the ice nearly every year and suppresses its variability. More broadly, where the Polar Front is located further away of the mean ice edge than at 170°E, such as for instance east and west of Drake Passage, it only limits the expansion in extreme cold years, setting a maximum extent but not restricting much the overall variability. Finally, the Polar Front has no impact on the variability of the ice edge in regions where it is too far north from the ice edge.

In the classical view, interannual variability of the sea ice cover is mainly constrained by atmospheric processes, while the ocean plays a larger role in decadal and longer trends (Bitz et al., 2005; Goosse and Zunz, 2014; Hobbs et al., 2016, Spira et al. 2026, Wilson et al., 2026). This seems a reasonable hypothesis for large-scale changes or integrated diagnostics, such as the sea ice extent. However, the ocean can also be a strong contributor at seasonal and interannual timescales, with for instance subsurface oceanic properties being critical in improving seasonal prediction of circumpolar sea ice extent (Dong et al., 2026). Our results demonstrate that the ocean controls the magnitude of the interannual variability of the ice edge position at the scale of a few hundreds of kilometers. Sea ice-ocean interactions, in particular associated with the presence of (sub-)mesoscale eddies, also modulates higher-frequency variations of the ice edge position and the dynamics of the Marginal Ice Zone (MIZ) (Gupta et al., 2024; Prend et al., 2025). Analyzing those processes requires fine resolution in both observations and models. Besides, this dominant oceanic contribution offers interesting perspectives for the predictability of ice edge position at scales on the order of one hundred kilometers, which is essential for ship routing but is notoriously difficult to achieve nowadays (Zampieri et al., 2019; Wagner et al., 2020; Massonnet et al., 2023; Zhao et al., 2024). As the oceanic impact may be more predictable a few days to weeks in advance than that of the atmosphere, models including adequate initialization and resolving the oceanic processes at those scales might thus be more skillful than low-resolution simulations.

https://doi.org/10.5194/egusphere-2026-1823
Preprint. Discussion started: 4 June 2026

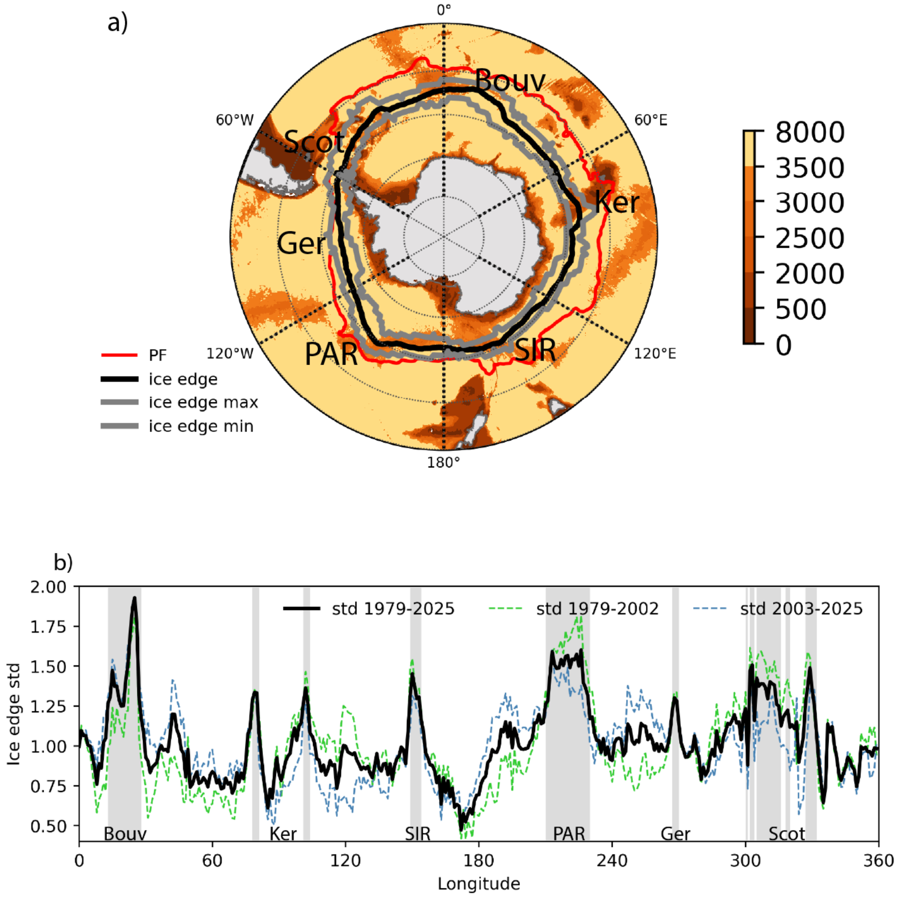

Fig. 1 a) Mean, minimum and maximum position the sea ice edge in September over the period 1979-2025. The red line is the position of the Polar Front (PF) following the definition of Park et al. (2019). The background colour represents the bathymetry (in m, Amante and Eakins, 2009). b) Standard deviation of the winter ice edge position for the period 1979-2025 (in °, black), the period 1979-2002 (dotted green) and the period 2003-2025 (dotted blue). The grey zones represent the longitude bands for which the standard deviation of the ice edge is larger than 1.2° for the period 1979-2025. 1.2° corresponds to the mean plus one standard deviation of the standard deviation of the winter ice edge position. The main nearby bathymetric features discussed in the text are also mentioned on both panels: Bouv (Bouvet Island and the western part of the Southwest Indian Ridge), Ker (Kerguelen Plateau), SIR (Southeast Indian Ridge), PAR (Pacific Antarctic Ridge), Ger (De Gerlache Seamont), Scot (Scotia ridge and South Sandwich Arch).

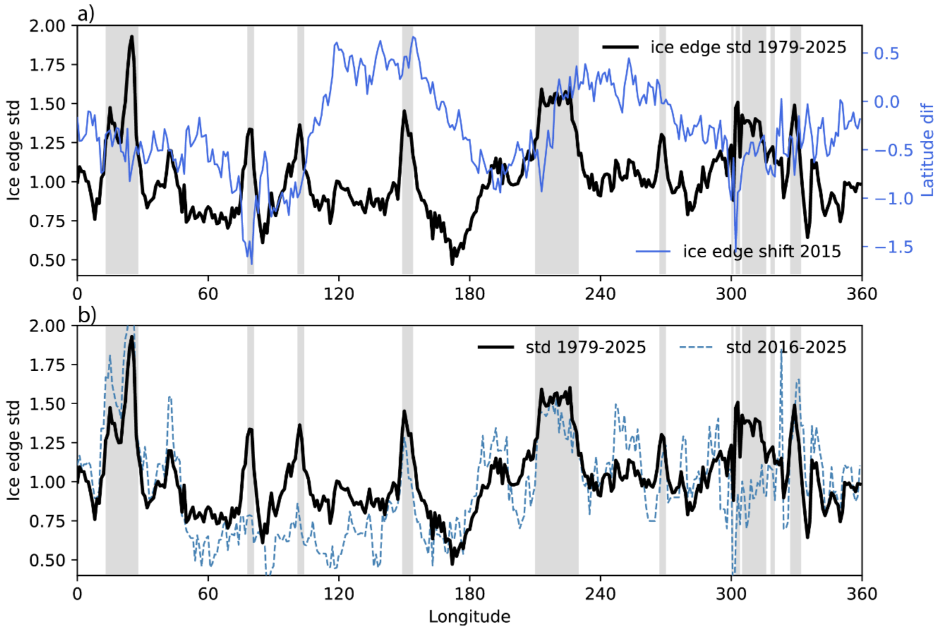

Fig. 2: Observed standard deviation of the September ice edge position for the period 1979-2025 (in °, black) and difference in the ice edge position between the period 1979-2015 and 2016-2025 (in °, blue). b) Comparison of the standard deviation of the ice edge position for the period 1979-2025 (in °, black) and for the period 2016-2025 (dotted blue). The grey zones represent the longitude bands for which the standard deviation of the ice edge is larger than 1.2°(i.e., mean plus one standard deviation) for the period 1979-2025.

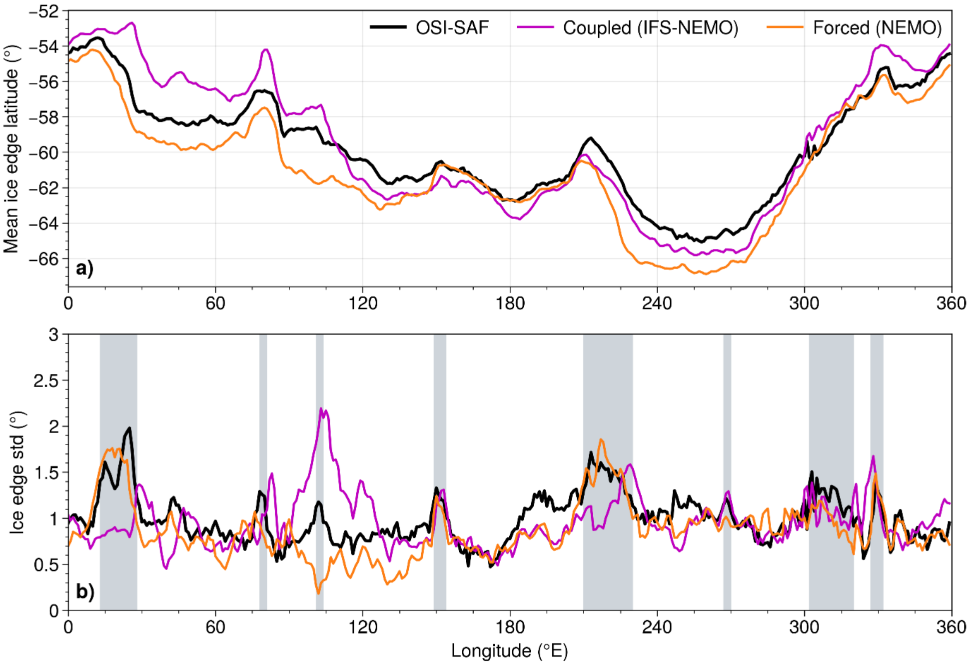

Fig 3. a) Mean position of the winter ice edge in observations (in °, black), in NEMO simulation forced by ERA5 (orange) over the period 1995-2024 and in IFS- NEMO over the last 30 years of the historical run (magenta). b) Standard deviation of the winter ice edge position (in °) over the same periods as the mean.

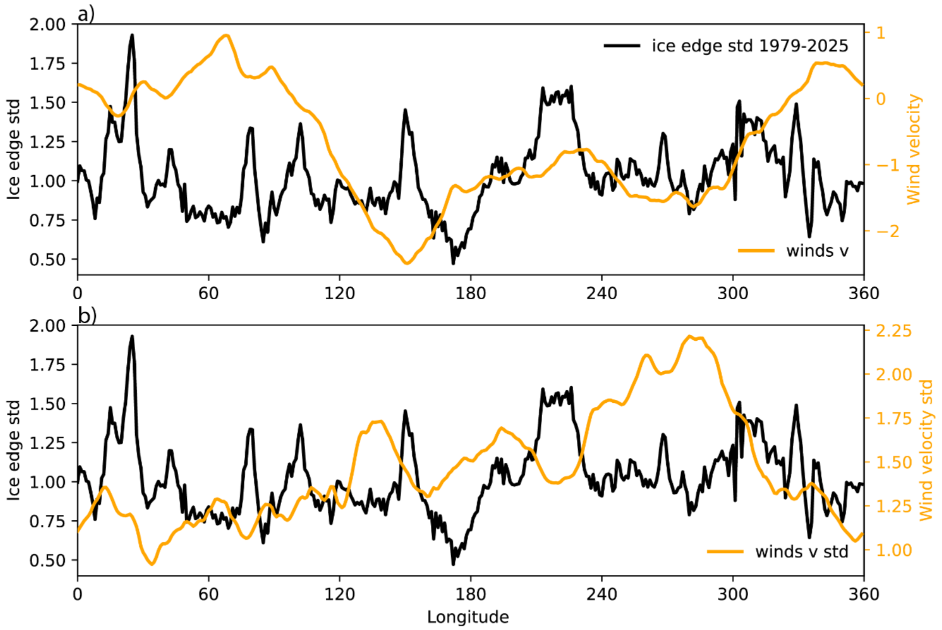

Fig. 4 Standard deviation of the winter ice edge position (in °, black) between 1979 and 2025 and a) the climatological mean meridional winds at 10m in September over the same period (positive for southerly winds) at 60°S (in m s^{-1}, orange) and b) the standard deviation of meridional winds at 60°S (in m s^{-1}, orange)

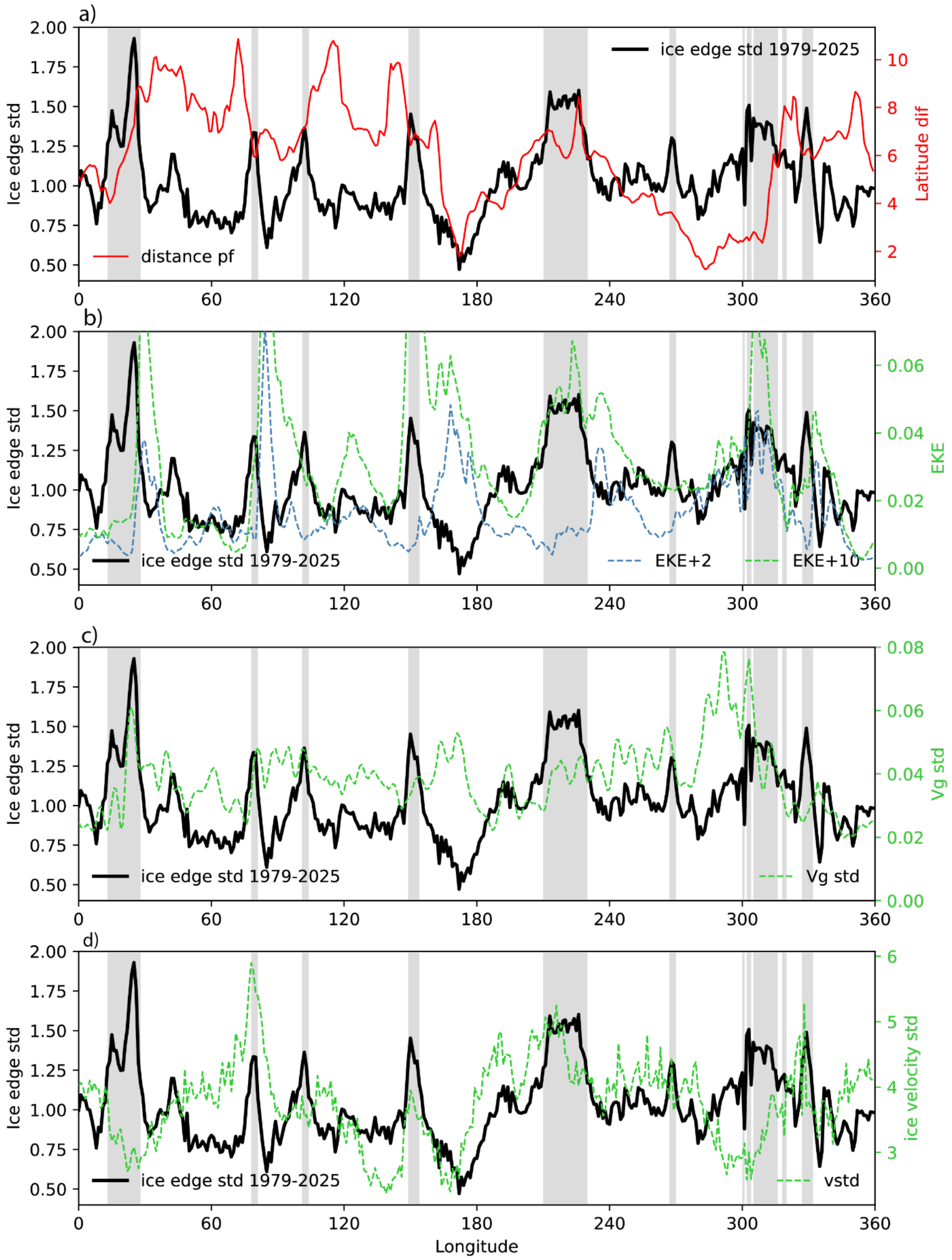

519

520

521

522

Fig 5. a) Standard deviation of the winter ice edge position for the period 1979-2025 (in °, black) and distance between the ice edge and the Polar Front (in °, red). b) Standard deviation of the winter ice edge position (in °, black) and mean Eddy Kinetic Energy (EKE, m^2s^{-2}) averaged derived from satellite observations (Auger et al. 2022) in the region 10° northward of the mean ice edge (m^2s^{-2}, in dotted green) and in the region 2° northward of the mean ice edge (m^2s^{-2}, in dotted blue). c) Standard deviation of the winter ice edge position (in °, black) and standard deviation of the mean meridional geostrophic velocity (Dragomir 2024) averaged over the region 5° northward and 5° southward of the mean ice edge ($m\ s^{-1}$, in dotted green). d) Standard deviation of the winter ice edge position (in °, black) and the standard deviation of the meridional sea ice velocity averaged in a band located from 5° south to 5° north of the mean ice edge position (in $cm\ s^{-1}$, dashed green). The grey zones represent the longitude bands for which the standard deviation of the ice edge is larger than 1.2° for the period 1979-2025.

https://doi.org/10.5194/egusphere-2026-1823
Preprint. Discussion started: 4 June 2026

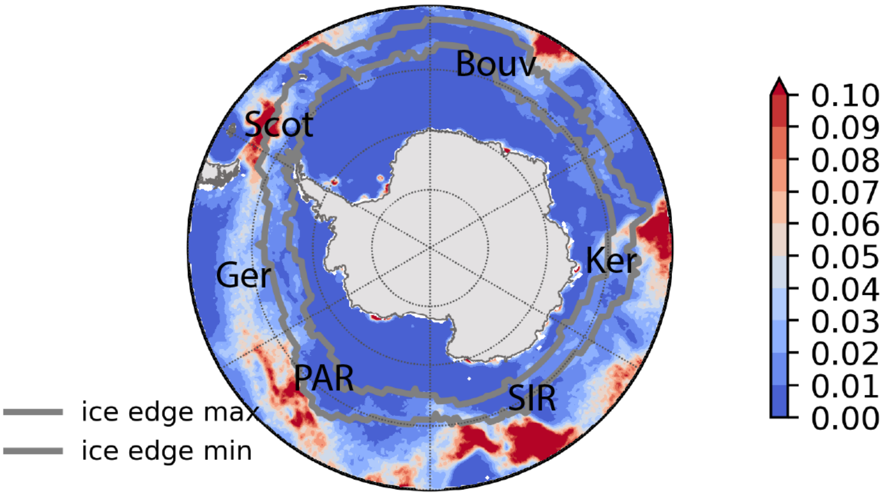

Fig 6. Minimum and maximum of the ice edge position in September over the period 1979-2025 with the mean Eddy Kinetic Energy (EKE, m^2s^{-2}) derived from satellite observations (Auger et al. 2022). The main nearby bathymetric features discussed in the text are also mentioned on both panels: Bouv (Bouvet Island and the western part of the Southwest Indian Ridge), Ker (Kerguelen Plateau), SIR (Southeast Indian Ridge), PAR (Pacific Antarctic Ridge), Ger (De Gerlache Seamont), Scot (Scotia ridge and South Sandwich Arch).

Data and code availability.

The OSI-SAF sea ice concentration data can be downloaded at https://osi-saf.eumetsat.int/products/osi-450 (last access: 15 November 2025) (1979–2015) and https://osi-saf.eumetsat.int/products/osi-430-b-complementing-osi-450 (last access: 15 November 2025) (2015 onwards). The ERA5 data is available from the Copernicus Climate Store: https://cds.climate.copernicus.eu/cdsapp#!/dataset/reanalysis-era5-single-levels-monthly-means?tab=overview(last access: 30 September 2024) (Hersbach et al., 2020b). NEMO and XIOS (a NEMO-compatible I/O library) are developed by the NEMO consortium (https://www.nemo-ocean.eu/, last access: 12 November 2025) and distributed under the CeCILL license (http://cecill.info/licences/Licence_CeCILL_V2-en.txt, last access: 12 November 2025). The bathymetric data has been taken from ETOP1 (NOAA National Geophysical Data Center, 2009, available at https://www.ncei.noaa.gov/access/metadata/landing-page/bin/iso?id=gov.noaa.ngdc.mgg.dem:316, last access: 1 September 2024). EKE Dataset is available on SEANOE with the https://doi.org/10.17882/81032 (Auger et al., 2021). The latitude of the fronts has been downloaded from https://australianantarcticdivision.github.io/orsifronts/articles/orsifronts.html#orsi-fronts-for-r (last access: 13 December 2024). The geosptrophic velocities come from Dragomir (2024) . [last access 15-09-2025]. The sea ice velocities are available at (Polar Pathfinder Daily 25 km EASE-Grid Sea Ice Motion Vectors, Version 4, last access 01-12-2025)

Author contributions. HG initiated the study and designed the analyses after discussions with all the co-authors. HG, CD, BR and DT performed the diagnostics. HG, CD and BR drew the figures. All the co-authors contributed in the interpretation of the results. HG wrote the initial version of the manuscript and the revisions, with inputs from all co-authors.

Competing interests. The contact author has declared that none of the authors has any competing interests.

Acknowledgments

We would like to thank Antoine Barthélemy for performing the simulation of NEMO driven by ERA5. Hugues Goosse is a Research Director within the F.R.S.-FNRS (Belgium). This work was performed in the framework of the PDR project T.0190.26 ‘Oceanic contribution to the multidecadal variability of Antarctic sea ice over the past two centuries’ of the FRS-FNRS. Computational resources were provided by the Center for High Performance Computing and Mass Storage (CISM) of the Université catholique de Louvain (UCLouvain) and the Consortium des Équipements de Calcul Intensif en Fédération Wallonie-Bruxelles (CÉCI), funded by the Fonds de la Recherche Scientifique de Belgique (F.R.S.-FNRS) under convention 2.5020.11 and by the Walloon Region. Alberto Naveira Garabato acknowledges U.K. Research and Innovation guarantee funding for a European Research Council Advanced Grant (EP/X025136/1). Benjamin Richaud is supported by the Belgian Science Policy Office (BELSPO) under the RESIST project (contract no. RT/23/RESIST). Alessandro Silvano acknowledges funding from NERC (NE/V014285/1). This work was supported by the TiPSOO (Tipping Points in the Southern Ocean Overturning) project, which is part of the ESA Climate Change Initiative (CCI). This publication is part of the EERIE project funded by the European Union (Grant Agreement No. 101081383). Views and opinions expressed are however those of the author(s) only and do not necessarily reflect those of the European Union or the European Climate Infrastructure and Environment Executive Agency (CINEA). Neither the European Union nor the granting authority can be held responsible for them. This work has received funding from the Swiss State Secretariat for Education, Research and Innovation (SERI) under contract #22.00366. This work was funded by UK Research and Innovation (UKRI) under the UK government’s Horizon Europe funding guarantee (grant nos. 10057890, 10049639, 10040510, 10040984).

References

Amante, C., and Eakins, B.W.: ETOPO1 1 Arc-Minute Global Relief Model: Procedures, Data Sources and Analysis, NOAA Technical Memorandum NESDIS NGDC-24, National Geophysical Data Center, NOAA. doi:10.7289/V5C8276M [access 29-01-2025], 2009.

Auger, M., Prandi, P., and Sallée, J.-B.: Daily Southern Ocean sea level anomaly and geostrophic currents from multimission altimetry, 2013-2019, SEANOE https://doi.org/10.17882/81032, 2021.

Auger M., Prandi, P. and Sallée, J.-B.: Southern Ocean sea level anomaly in the sea ice-covered sector from multimission satellite observations. Scientific Data 9,70, https://doi.org/10.1038/s41597-022-01166-z 1, 2022.

Bitz, C. M., Holland, M. M., Hunke, E. C., and Moritz, R. E.: Maintenance of the sea-ice edge, J. Clim., 18(15), 2903–2921, https://doi.org/10.1175/JCLI3428.1, 2005.

Blanchard-Wrigglesworth, E., Roach, L. A., Donohoe, A., and Ding, Q.: Impact of winds and Southern Ocean SSTs on Antarctic sea ice trends and variability, J. Clim., 34, 1–47, https://doi.org/10.1175/JCLI-D-20-0386.1, 2021.

Boehm, C.L., Thompson, D. W. J., and Blanchard-Wrigglesworth, E.: The key role of the Southern Annular Mode during the sea-ice maximum for Antarctic sea ice and its recent loss, Com. Earth & Environment, 6, 833, https://doi.org/10.1038/s43247-025-02792-2, 2025

Cai, Y., Lei, R., Chen, D., du Plessis, M., Liu, C., Han, X., Wu, L.: Anticyclonic component of eddy dipoles traps sea ice within the Marginal Ice Zone, J. Geophys. Res.: Oceans 130, e2025JC022426. https://doi.org/10.1029/2025JC022426, 2025

Diamond, R., Sime, L. C., Holmes, C. R., and Schroeder, D.: CMIP6 models rarely simulate Antarctic winter sea-ice anomalies as large as observed in 2023, Geophys. Res. Let., 51, e2024GL109265. https://doi.org/10.1029/2024GL109265, 2024

Doblas-Reyes, F. J., Kontkanen, J., Sandu, I., Acosta, M., Al Turjmam, M. H., Alsina-Ferrer, I., Andrés-Martínez, M., Arriola, L., Axness, M., Batlle Martín, M., Bauer, P., Becker, T., Beltrán, D., Beyer, S., Bockelmann, H., Bretonnière, P.-A., Cabaniols, S., Caprioli, S., Castrillo, M., Chandrasekar, A., Cheedela, S., Correal, V., Danovaro, E., Davini, P., Enkovaara, J., Frauen, C., Früh, B., Gaya Àvila, A., Ghinassi, P., Ghosh, R., Ghosh, S., González, I., Grayson, K., Griffith, M., Hadade, I., Haine, C., Hartick, C., Haus, U.-U., Hearne, S., Järvinen, H., Jiménez, B., John, A., Juchem, M., Jung, T., Kegel, J., Kelbling, M., Keller, K., Kinoshita, B., Kiszler, T., Klocke, D., Kluft, L., Koldunov, N., Kölling, T., Kolstela, J., Kornblueh, L., Kosukhin, S., Lacima-Nadolnik, A., Leal Rojas, J. J., Lehtiranta, J., Lunttila, T., Luoma, A., Manninen, P., Medvedev, A., Milinski, S., Mohammed, A. O. A., Müller, S., Naryanappa, D., Nazarova, N., Niemelä, S., Niraula, B., Nortamo, H., Nummelin, A., Nurisso, M., Ortega, P., Paronuzzi, S., Pedruzo Bagazgoitia, X., Pelletier, C., Peña, C., Polade, S., Pradhan, H., Quintanilla, R., Quintino, T., Rackow, T., Räisänen, J., Rajput, M. M., Redler, R., Reuter, B., Rocha Monteiro, N., Roura-Adserias, F., Ruppert, S., Sayed, S., Schnur, R., Sharma, T., Sidorenko, D., Sievi-Korte, O., Soret, A., Steger, C., Stevens, B., Streffing, J., Sunny, J., Tenorio, L., Thober, S., Tigerstedt, U., Tinto, O., Tonttila, J., Tuomenvirta, H., Tuppi, L., Van Thielen, G., Vitali, E., von Hardenberg, J., Wagner, I., Wedi, N., Wehner, J., Willner, S., Yepes-Arbós, X., Ziemen, F., and Zimmermann, J.: The Destination Earth digital twin for climate change adaptation, EGUsphere [preprint], doi:10.5194/egusphere-2025-2198.d, 2025.

Dong, X., Massonnet, F., Nie, Y., Richaud, B., Gao, Y., Hoffman, L., Wang, Y , and Yang Q.: Incorporating subsurface oceanic variables improves seasonal Antarctic sea ice prediction with neural networks, J. Geophys. Res.: Atmos., 131, e2025JD045470. https://doi.org/10.1029/2025JD045470, 2026

Dragomir, O. C.: Gridded altimetric dynamic ocean topography for the Southern Ocean, University of Southampton, doi.org/10.5258/SOTON/D3006 [last access 15-09-2025], 2024

Dufour, C.O., Griffies, S.M., de Souza, G.F., Frenger, I., Morrison, A.K., Palter, J.B., Sarmiento, J.L., Galbraith, E.D., Dunne, J.D., Anderson, W.G., Slater, R.D.: Role of Mesoscale Eddies in Cross-Frontal Transport of Heat and Biogeochemical Tracers in the Southern Ocean, J. Phys. Ocean., 45, 3057-3081, https://doi.org/10.1175/JPO-D-14-0240.1, 2015

Eabry, M.D., Goyal, R., Taschetto, A.S., Hobbs, W., and Gupta A.S.: Combined impacts of Southern Annular Mode and Zonal Wave 3 on Antarctic sea ice variability, J. Clim. 37, 1759-1775. DOI: https://doi.org/10.1175/JCLI-D-23-0516.1, 2025.

Eayrs, C., Holland, D. M., Francis, D., Wagner, T. J. W., Kumar, R., and Li, X.: Understanding the seasonal cycle of Antarctic sea ice extent in the context of longer-term variability, Rev. Geophys., 57, 1037–1064, https://doi.org/10.1029/2018RG000631, 2019.

Edholm, J. M., du Plessis, M. D., Biddle, L. C., Gille, S. T., Mazloff, M. R., Rosenthal, H. S., and Swart, S.: From synoptic to submesoscale: Understanding sensible heat flux variability in the Southern Ocean, J. Geophys. Res.: Oceans, 130, e2024JC022292. https://doi.org/10.1029/2024JC022292, 2025

Eisenman, I.: Geographic muting of changes in the Arctic sea ice cover, Geophys.Res. Lett., 37, L16501, doi:10.1029/2010GL043741, 2010.

Espinosa, Z.I., Blanchard-Wrigglesworth, E. and Bitz, C. M.: Understanding the drivers and predictability of record low Antarctic sea ice in austral winter 2023, Com. Earth & Environment, 5,723, https://doi.org/10.1038/s43247-024-01772-2, 2024.

Eyring, V., Bony, S., Meehl, G. A., Senior, C. A., Stevens, B., Stouffer, R. J., and Taylor, K. E.: Overview of the Coupled Model Intercomparison Project Phase 6 (CMIP6) experimental design and organization, Geosci. Model Dev., 9, 1937–1958, https://doi.org/10.5194/gmd-9-1937-2016, 2016.

Ferola, A. I., Cotroneo, Y., Wadhams, P., Fusco, G., Falco, P., Budillon, G., and Aulicino, G.: The role of the Pacific-Antarctic Ridge in establishing the northward extent of Antarctic sea-ice. Geophys. Res. Let., 50, e2023GL104373. https://doi.org/10.1029/2023GL104373, 2023.

Ferreira D., Marshall J, Bitz CM, Solomon S, and Plumb, A.: Antarctic Ocean and sea ice response to ozone depletion: a two time- scale problem, J. Clim., 28,1206–1226, doi:10.1175/JCLI-D-14-00313.1, 2015

Goosse, H., Arzel, O., Bitz, C.M., de Montety, A. and Vancoppenolle, M.: Increased variability of the Arctic summer ice extent in a warmer climate, Geophys. Res. Let., 36, L23702, doi:10.1029/2009GL040546, 2009.

Goosse, H. and Zunz, V.: Decadal trends in the Antarctic sea ice extent ultimately controlled by ice-ocean feedback, The Cryosphere, 8, 453–470, Doi: 10.5194/tc-8-453-2014, 2014.

Goosse H., Allende Contador, S., Bitz, C., Blanchard-Wrigglesworth, E., Eayrs, C., Fichefet, T., Himmich, K., Huot, P-V., Klein, F., Marchi, S., Massonnet, F., Mezzina, B., Pelletier, C., Roach, L., Vancoppenolle, M., and van Lipzig, N.: Modulation of the seasonal cycle of the Antarctic sea ice extent by sea ice processes and feedbacks with the ocean and the atmosphere, The Cryosphere, 19, 5763–5779, https://doi.org/10.5194/tc-19-5763-2025, 2023.

https://doi.org/10.5194/egusphere-2026-1823
Preprint. Discussion started: 4 June 2026

Goosse, H., Libera, S., Naveira Garabato, A. C., Richaud, B., Silvano, A., and Vancoppenolle, M.: Winter sea ice edge shaped by Antarctic Circumpolar Current pathways, The Cryosphere, 19, 5763–5779, https://doi.org/10.5194/tc-19-5763-2025, 2025.

Gupta, M., Gürcan, E., and Thompson, A. F.: Eddy-induced dispersion of sea ice floes at the marginal ice zone, Geophys. Res. Let., 51, e2023GL105656. https://doi.org/10.1029/2023GL105656, 2024

Haarsma, R. J., Roberts, M. J., Vidale, P. L., Senior, C. A., Bellucci, A., Bao, Q., Chang, P., Corti, S., Fučkar, N. S., Guemas, V., von Hardenberg, J., Hazeleger, W., Kodama, C., Koenigk, T., Leung, L. R., Lu, J., Luo, J.-J., Mao, J., Mizielinski, M. S., Mizuta, R., Nobre, P., Satoh, M., Scoccimarro, E., Semmler, T., Small, J., and von Storch, J.-S.: High Resolution Model Intercomparison Project (HighResMIP v1.0) for CMIP6, Geosci. Model Dev., 9, 4185–4208, https://doi.org/10.5194/gmd-9-4185-2016, 2016.

Haumann, F. A., Gruber, N., Munnich, M., Frenger, I., and Kern, S.: Sea-ice transport driving southern ocean salinity and its recent trends. Nature, 537(7618), 89–92. https://doi.org/10.1038/nature19101, 2016.

Hausmann, U., McGillicuddy, D. J., and Marshall, J.: Observed mesoscale eddy signatures in Southern Ocean surface mixed-layer depth, J. Geophys. Res. Oceans, 122, 617–635, doi:10.1002/2016JC012225, 2017.

Hersbach, H., Bell, B., Berrisford, P., Hirahara, S., Horányi, A., Muñoz-Sabater, J., Nicolas, J., Peubey, C., Radu, R., Schepers, D., Simmons, A., Soci, C., Abdalla, S., Abellan, X., Balsamo, G., Bechtold, P., Biavati, G., Bidlot, J., Bonavita, M., De Chiara, G., Dahlgren, P., Dee, D., Diamantakis, M., Dragani, R., Flemming, J., Forbes, R., Fuentes, M., Geer, A., Haimberger, L., Healy, S., Hogan, R. J., Hólm, E., Janisková, M., Keeley, S., Laloyaux, P., Lopez, P., Lupu, C., Radnoti, G., de Rosnay, P., Rozum, I., Vamborg, F., Villaume, S., and Thépaut, J.-N.: The ERA5 global reanalysis, Q. J. Roy. Meteor. Soc., 146, 1999–2049, https://doi.org/10.1002/qj.3803, 2020a.

Hersbach, H., Bell, B., Berrisford, P., Hirahara, S., Horányi, A., Muñoz-Sabater, J., Nicolas, J., Peubey, C., Radu, R., Schepers, D., Simmons, A., Soci, C., Abdalla, S., Abellan, X., Balsamo, G., Bechtold, P., Biavati, G., Bidlot, J., Bonavita, M., De Chiara, G., Dahlgren, P., Dee, D., Diamantakis, M., Dragani, R., Flemming, J., Forbes, R., Fuentes, M., Geer, A., Haimberger, L., Healy, S., Hogan, R. J., Hólm, E., Janisková, M., Keeley, S., Laloyaux, P., Lopez, P., Lupu, C., Radnoti, G., De Rosnay, P., Rozum, I., Vamborg, F., Villaume, S., and Thépaut, J. N.: ERA5 hourly data on pressure levels from 1940 to present, Copernicus Climate Change Service (C3S) Climate Data Store (CDS) [data set], https://cds.climate.copernicus.eu/cdsapp#!/dataset/reanalysis-era5-single-levels?tab=overview (last access: 30 September 2024), 2020b.

Himmich, K., Vancoppenolle, M., Madec, G., Sallée, J.-B., Holland, P. R., and Lebrun, M.: Drivers of Antarctic sea ice advance. Nature Communications 14, 6219, https://doi.org/10.1038/s41467-023-41962-8, 2023.

Hobbs, W. R., Massom, R., Stammerjohn, S., Reid, P., Williams, G., and Meier, W.: A review of recent changes in Southern Ocean sea ice, their drivers and forcings, Glob. Planet. Change, 143, 228-250, 10.1016/j.gloplacha.2016.06.008, 2016.

Hobbs, W., Spence, P., Meyer, A., Schroeter, S., Fraser, A. D., Reid, P., Tian, T. R., Wang, Z., Liniger, G., Doddridge, E. W., and Boyd, P. W: Observational evidence for a regime shift in summer Antarctic sea ice. Journal of Climate DOI 10.1175/JCLI-D-23-0479.1, 2024.

Holland, P. R., and Kimura, N.: Observed concentration budgets of Arctic and Antarctic Sea ice. J. Clim., 29, 5241–5249, https://doi.org/10.1175/JCLI-D-16-0121.1, 2016

Jena, B., Kshitija, S., Bajish, C. C., Turner, J., Holmes, C., Wilkinson, J., Mohan, R. , and Thamban, M. , : Evolution of Antarctic sea ice ahead of the record low annual maximum extent in September 2023. Geophys. Res. Le., 51, e2023GL107561, https://doi.org/10.1029/2023GL107561, 2024

Kusahara, K. and Tatebe, H.: Causes of the abrupt and sustained 2016–2023 Antarctic sea-ice decline: A sea ice–ocean model perspective, Geophys. Res. Lett., 52, e2025GL115256, https://doi.org/10.1029/2025GL115256, 2025.

Kwok, R., Pang, S. S., and Kacimi, S.: Sea ice drift in the southern ocean: Regional patterns, variability, and trends, Elementa: Science of the Anthropocene, 5, 32. https://doi.org/10.1525/elementa.226, 2017.

Lefebvre, W., and Goosse, H.: An analysis of the atmospheric processes driving the large-scale winter sea-ice variability in the Southern Ocean, J. Geophys. Res., 113, C02004, doi:10.1029/2006JC004032, 2008.

Lavergne, T., Sørensen, A. M., Kern, S., Tonboe, R., Notz, D., Aaboe, S., Bell, L., Dybkjær, G., Eastwood, S., Gabarro, C., Heygster, G., Killie, M. A., Brandt Kreiner, M., Lavelle, J., Saldo, R., Sandven, S., and Pedersen, L. T.: Version 2 of the EUMETSAT OSI SAF and ESA CCI sea-ice concentration climate data records, The Cryosphere, 13, 49–78, https://doi.org/10.5194/tc-13-49-2019, 2019.

Li, S., Cai, W., and Wu, L.: Attenuated interannual variability of austral winter Antarctic sea ice over recent decades, Geophys. Res. Let., 47, e2020GL090590. https://doi.org/10.1029/2020GL090590, 2020

Madec, G., and the NEMO team: NEMO ocean engine (v4.0), Notes du Pôle de modélisation de l'Institut Pierre-Simon Laplace (IPSL), No. 27, Zenodo, https://doi.org/10.5281/zenodo.3878122, 2019

Madec, G. and the NEMO System Team.: NEMO Ocean Engine Reference Manual, Zenodo, https://doi.org/10.5281/zenodo.8167700, 2023.

Manucharyan, G. E., and Thompson, A. F.: Submesoscale sea ice-ocean interactions in marginal ice zones, J. Geophys. Res.: Oceans 122, 9455-9475, https://doi.org/10.1002/2017JC012895, 2017.

Martinson, D. G.: Evolution of the Southern-Ocean winter mixed layer and sea ice - open ocean deep-water formation and ventilation. J. Geophys. Res.:Oceans, 95, 11641-11654, 10.1029/Jc095ic07p11641, 1990.

Martinson, D.G.: Antarctic circumpolar current's role in the Antarctic ice system: An overview, Palaeogeography, Palaeoclimatology, Palaeoecology, 335-336, 71–74, doi:10.1016/j.palaeo.2011.04.007,2012.

Massonnet, F., Barreira, S., Barthélemy, A., Bilbao, R., Blanchard-Wrigglesworth, E., Blockley, E., Bromwich, D.H., Bushuk, M., Dong, X., Goessling, H.F., Hobbs, W., Iovino, D., Lee, W.-S., Li, C., Meier, W.N., Merryfield, W.J., Moreno-Chamarro, E., Morioka, Y., Li, X., Niraula, B., Petty, A., Sanna, A., Scilingo, M., Shu, Q., Sigmond, M., Sun, N., Tietsche, S., Wu, X., Yang, Q., and Yuan, X.: SIPN South: six years of coordinated seasonal Antarctic sea ice predictions, Front. Mar. Sci., 10:1148899, doi: 10.3389/fmars.2023.1148899, 2023

Morrison, A. K., Griffies, S. M., Winton, M., Anderson, W. G., and Sarmiento, J. L.: Mechanisms of Southern Ocean heat uptake and transport in a global eddying climate model, J. Climate, 29, 2059–2075, https://doi.org/10.1175/JCLI-D-15-0579.1, 2016.

Nakamura, H., and Shimpo, A.: Seasonal variations in the Southern Hemisphere storm tracks and jet streams as revealed in a reanalysis dataset, J. Clim., 17, 1828–1844, DOI: https://doi.org/10.1175/1520-0442(2004)017<1828:SVITSH>2.0.CO;2, 2004

NOAA National Geophysical Data Center: ETOPO1 1 Arc-Minute Global Relief Model, NOAA National Centers for Environmental Information, Accessed [29-01-2025], 2009.

OSI SAF: Global Sea Ice Concentration Climate Data Record v2.0 - Multimission, EUMETSAT SAF on Ocean and Sea Ice, http://dx.doi.org/10.15770/EUM_SAF_OSI_0008, 2017.

Park, Y.-H., Park, T., Kim, T.-W., Lee, S.-H., Hong, C.-S., Lee, J.-H., Rio, M.-H., Pujol, M.-I., Ballarotta, M., Durand, I., and Provost, C.: Observations of the Antarctic Circumpolar Current over the Udintsev Fracture Zone, the narrowest choke point in the Southern Ocean, J. Geophys. Res.: Oceans, 124, 4511–4528, https://doi.org/10.1029/2019JC015024, 2019.

Parkinson, C.L., and Cavalieri, D.J.: Antarctic sea ice variability and trends, 1979–2010, The Cryosphere, 6, 871–880. http://dx.doi.org/10.5194/Tc-6-871-2012, 2012

Parkinson, C.L.: Global sea ice coverage from satellite data: annual cycle and 35-Yr trends, J. Clim., 27, 9377-9382, DOI: 10.1175/JCLI-D-14-00605.1, 2014

Parkinson, C.L., and DiGirolamo, N.E.: Sea ice extents continue to set new records: Arctic, Antarctic, and global results, Remote Sensing of Environment, 267, 112753. https://doi.org/10.1016/j.rse.2021.112753, 2021.

Prend, C.J., Swart, S., Stewart, A. L., du Plessis, M. D., Manucharyan, G. E. and Thompson, A. F.: Observed regimes of submesoscale dynamics in the Southern Ocean seasonal ice zone, Nat. Communications, 16, 8344. https://doi.org/10.1038/s41467-025-63775-7, 2025.

Purich, A., and Doddridge, E.W.: Record low Antarctic sea ice coverage indicates a new sea ice state, Commun. Earth Environ., 4, 314, https://doi.org/10.1038/s43247-023-00961-9, 2023.

Rackow, T., Pedruzo-Bagazgoitia, X., Becker, T., Milinski, S., Sandu, I., Aguridan, R., Bechtold, P., Beyer, S., Bidlot, J., Boussetta, S., Deconinck, W., Diamantakis, M., Dueben, P., Dutra, E., Forbes, R., Ghosh, R., Goessling, H. F., Hadade, I., Hegewald, J., Jung, T., Keeley, S., Kluft, L., Koldunov, N., Koldunov, A., Kölling, T., Kousal, J., Kühnlein, C., Maciel, P., Mogensen, K., Quintino, T., Polichtchouk, I., Reuter, B., Sármány, D., Scholz, P., Sidorenko, D., Streffing, J., Sützl, B., Takasuka, D., Tietsche, S., Valentini, M., Vannière, B., Wedi, N., Zampieri, L., and Ziemen, F.: Multi-year simulations at kilometre scale with the Integrated Forecasting System coupled to FESOM2.5 and NEMOv3.4, Geosci. Model Dev., 18, 33–69, https://doi.org/10.5194/gmd-18-33-2025, 2025.

Raphael, M. N.: The influence of atmospheric zonal wave three on Antarctic sea ice variability, J. Geophys. Res., 112, D12112, doi:10.1029/2006JD007852, 2007

Raphael, M.N., Maierhofer, T.J., Fogt, R.L., Hobbs W.R., and Handcock M.S.: A twenty-first century structural change in Antarctica's sea ice system, Commun. Earth Environ., 6, 131, https://doi.org/10.1038/s43247-025-02107-5, 2025

Richaud, B., Massonnet, F., Fichefet, T., Topál, D., Barthélemy, A., and Docquier, D.: Anatomy of Arctic and Antarctic sea ice lows in an ocean–sea ice model, The Cryosphere, 20, 791–810, https://doi.org/10.5194/tc-20-791-2026, 2026

Rintoul S.R.: The global influence of localized dynamics in the Southern Ocean, Nature, 558, 209–218. https://doi.org/10.1038/s41586-018-0182-3, 2018.

Roach, C. J., and Speer, K.: Exchange of water between the Ross Gyre and ACC assessed by Lagrangian particle tracking, J. Geophys. Res.: Oceans, 124, 4631–4643. https://doi.org/10.1029/2018JC014845, 2019.

Roach, L. A., Dörr, J., Holmes, C. R., Massonnet, F., Blockley, E. W., Notz, D., Rackow, T., Raphael, M.N., O'Farrell, S. P., Bailey, D.A., Bitz, C.M.: Antarctic sea ice area in CMIP6. Geophysical Research Letters, 47, e2019GL086729. https://doi.org/10.1029/2019GL086729, 2020.

Roberts, M. J., Reed, K. A., Bao, Q., Barsugli, J. J., Camargo, S. J., Caron, L.-P., Chang, P., Chen, C.-T., Christensen, H. M., Danabasoglu, G., Frenger, I., Fučkar, N. S., Hasson, S. U., Hewitt, H. T., Huang, H., Kim, D., Kodama, C., Lai, M., Leung, L.-Y. R., Mizuta, R., Nobre, P., Ortega, P., Paquin, D., Roberts, C. D., Scoccimarro, E., Seddon, J., Treguier, A. M., Tu, C.-Y., Ullrich, P. A., Vidale, P. L., Wehner, M. F., Zarzycki, C. M., Zhang, B., Zhang, W., and Zhao, M.: High Resolution Model Intercomparison Project phase 2 (HighResMIP2) towards CMIP7, Geosci. Model Dev., 18, 1307–1332, https://doi.org/10.5194/gmd-18-1307-2025, 2025.

Sallée, J. B., Speer, K. and Rintoul, S.R.: Mean-flow and topography control on surface eddy-mixing in the Southern Ocean, J. Mar. Res., 69, 753–777, https://elischolar.library.yale.edu/journal_of_marine_research/326, 2011.

Schlosser, E., Haumann, F. A., and Raphael, M. N.: Atmospheric influences on the anomalous 2016 Antarctic sea ice decay, The Cryosphere, 12, 1103–1119, https://doi.org/10.5194/tc-12-1103-2018, 2018

Silvano, A., Narayanan, A., Catany, R., and Naveira Garabato, A.C. : Rising surface salinity and declining sea ice: A new Southern Ocean state revealed by satellites, 122 (27) e2500440122, https://doi.org/10.1073/pnas.2500440122, 2025.

Spira, T., du Plessis, M., Haumann, F.A., Giddy, I., Narayanan, A., Silvano, A., and Swart, S.: Wind-triggered Antarctic sea-ice decline preconditioned by thinning Winter Water. Nat. Clim. Chang, https://doi.org/10.1038/s41558-026-02601-4, 2026.

Stammerjohn, S. E., Martinson, D. G., Smith, R. C., Yuan, X., and Rind, D.; Trends in Antarctic annual sea ice retreat and advance and their relation to El Niño–Southern Oscillation and Southern Annular Mode variability, J. Geophys. Res., 113, C03S90, https://doi.org/10.1029/2007JC004269, 2008.

Thompson, A. F., and Sallée, J.-B.: Jets and topography: Jet transitions and the impact on transport in the Antarctic Circumpolar Current, J. Phys. Oceanogr., 42, 956–972, https://doi.org/10.1175/JPO-D-11-0135.1, 2012.

Tschudi, M., W. N. Meier, J. S. Stewart, C. Fowler, and J. Maslanik.: Polar Pathfinder Daily 25 km EASE-Grid Sea Ice Motion Vectors, Version 4. [subset NSIDC-0116], Boulder, Colorado USA. NASA National Snow and Ice Data Center Distributed Active Archive Center. https://doi.org/10.5067/INAWUWO7QH7B. [Last Access 01-12-2025], 2019.

Turner, J., Phillips, T., Marshall, G. J., Hosking, J. S., Pope, J. O., Bracegirdle, T. J., and Deb, P.: Unprecedented springtime retreat of Antarctic sea ice in 2016, Geophys. Res. Lett., 44, 6868–6875, https://doi.org/10.1002/2017GL073656, 2017.

Vancoppenolle, M., Rousset, C., Blockley, E., and the NEMO Sea Ice Working Group: SI3 – Sea Ice modelling Integrated Initiative – The NEMO Sea Ice Engine, Zenodo, https://doi.org/10.5281/zenodo.7534900, 2023.

Wagner P.M., N. Hughes, P. Bourbonnais, J. Stroeve, L. Rabenstein, U. Bhatt, J. Little, H. Wiggins & A. Fleming: Sea ice information and forecast needs for industry maritime stakeholders, Polar Geography, 43, 160-187, DOI: 10.1080/1088937X.2020.1766592, 2020.

Wang, J., Massonnet, F., Goosse, H., Luo, H., Barthélemy, A. and Yang, Q.: Synergistic atmosphere-ocean-ice influences have driven the 2023 all-time Antarctic sea-ice record low, Commun. Earth Environ., 5, 415, https://doi.org/10.1038/s43247-024-01523-3, 2024.

Wilson, E.A., Lexi Arlen, L., and Campbell, E.C.: Recent extremes in Antarctic sea ice extent modulated by ocean heat ventilation, Proc. Nat. Acad. Sc., 123 (14) e2530832123, https://doi.org/10.1073/pnas.2530832123, 2026.

Yuan, X., and Martinson, D. G.: The Antarctic dipole and its predictability. Geophys. Res. Let., 28, 3609–3612, https://doi.org/10.1029/2001GL012969, 2001.

Zampieri, L., Goessling, H. F., and Jung, T.: Predictability of Antarctic sea ice edge on subseasonal time scales. Geophys. Res. Let., 46, 9719–9727. https://doi.org/10.1029/2019GL084096, 2019

Zhan, X, and Chen, L.: Climatology and changes in extratropical cyclone activity in the Southern Hemisphere during austral winters from 1948 to 2017, .J. Applied Meteor. Clim., 62, 971-983, 2023.

Zhang, L., Ren, X., Wang, C.-Y., Gan, B., Wu, L.,·and Cai, W: An observational study on the interactions between storm tracks and sea ice in the Southern Hemisphere, Clim. Dyn, 62, 17–36, https://doi.org/10.1007/s00382-023-06894-5, 2024

Zhao, F, Liang, X., Tian, Z., Li, M., Liu, N., and Liu, C.: Southern Ocean ce Prediction System version 1.0 (SOIPS v1.0): description of the system and evaluation of synoptic-scale sea ice forecasts, Geosci. Model Dev., 17, 6867–6886, https://doi.org/10.5194/gmd-17-6867-2024, 2024.

Zunz, V., Goosse, H., and Massonnet, F.: How does internal variability influence the ability of CMIP5 models to reproduce the recent trend in Southern Ocean sea ice extent?, The Cryosphere, 7, 451–468, https://doi.org/10.5194/tc-7-451-2013, 2013.